UVC-induced degradation of cilastatin in natural water and treated wastewater

UVC-induced direct photolysis as an efficient process for the degradation of cilastatin in natural and waste water

Nicoleta Solomou[1], Marco Minella[2], Davide Vione[2,*], Elefteria Psillakis[1,*]

[1] Laboratory of Aquatic Chemistry, School of Environmental Engineering, Technical University of Crete, GR-73100, Chania, Crete, Greece

[2] Department of Chemistry, University of Torino, Via P. Giuria 5, 10125 Torino, Italy.

Abstract

This work reports for the first time the UVC photodegradation of cilastatin, a renal dehydropeptidase inhibitor co-adminstered with the imipenem antibiotic. Initially, solutions of cilastatin at varying concentrations were prepared in ultra-pure water and the direct photolysis of cilastatin was monitored under 254-nm irradiation. Degradation was slower at higher initial cilastatin concentrations, due to absorption saturation. Of the different eluting photoproducts, only one was tentatively identified as oxidized cilastatin bearing a sulfoxide group. UV-254 photolysis occurred faster at lower pH values, because the protonated forms of the molecule (H_3A^+, H_2A) have both higher absorption coefficients and higher photolysis quantum yields than the non-protonated ones (HA^-, A^{2-}). The direct photolysis of cilastatin does not involve $^{\bullet}OH$, as excluded by experiments in which t-butanol was added as $^{\bullet}OH$

scavenger, whereas the presence of humic acids inhibited photolysis due to competition for radiation absorption. The same explanation partially accounts for the observation that the photolysis kinetics of cilastatin was slower in tap water, river water and treated wastewater samples compared to ultra-pure water. Moreover, the direct photolysis quantum yield was also lower in water matrices compared to ultra-pure water. Similar findings reported for triclosan and the herbicide 2-methyl-4-chlorophenoxyacetic acid in previous studies might suggest that the water matrix components could carry out either physical quenching of cilastatin's excited states or back-reduction to cilastatin of the partially oxidized degradation intermediates. Overall, the present results demonstrate that UVC irradiation is a fast and efficient process for the degradation of cilastatin in natural water and wastewater.

Keywords: cilastatin; carbapenems; antibiotics; direct photolysis; waste water tertiary treatments; UVC photolysis.

1. Introduction

Antibiotics are frequently used in the treatment and prevention of infectious disease, as well as to treat humans and animals. Imipenem was the first member of the carbapenem class of antibiotics and an important broad-spectrum β-lactam antibiotic, often used as a "last-line antibiotic" when patients with infections became gravely ill or were suspected of harboring resistant bacteria (Proia et al., 2018; Reina et al., 2018; Briones et al., 2020). At early stages of development when imipenem was administered alone, low urinary recovery in animals and human volunteers were recorded, and further toxicological studies reported proximal tubular necrosis to rabbits (Drusano et al., 1984). The concept of co-administering imipenem together with a renal dehydropeptidase inhibitor to improve the urinary antibiotic profile resulted in the synthesis and use of cilastatin. The combination of imipenem and cilastatin in a ratio of 1:1 yielded high urinary concentrations of imipenem (recoveries increased from 12-42% to 70% of the dose when co-administered with cilastatin), and in addition, cilastatin prevented entry of imipenem into the proximal tubular epithelium (Hutt and O'Grady, 1996). At the same time, the urinary recoveries of cilastatin in the presence or absence of imipenem were reported to range between 70-80% after 6 h from administration (Norrby et al., 1984; Hsieh et al., 1985).

In recent years, the consumption of last-line antibiotics has been rapidly increasing across all income groups (Yılmaz and Özcengiz, 2017; Klein et al., 2018). In particular, the increased consumption of carbapenems such as imipenem, has resulted in their environmental release through various routes such as patients' excretions, hospital wastewater and the pharmaceutical industry (Cheng et al., 2015; Szekeres et al., 2017) and in their widespread occurrence in aquatic systems (Tran et al., 2016; Szekeres et al., 2017; Proia et al., 2018). The latter findings were assumed to account for the developed resistance of some Gram-negative bacteria to carbapenems (Kumarasamy et al., 2010), which is now spreading throughout the

65 world and is threatening the efficiency of this essential class of life-saving antibiotics (Papp-
66 Wallace et al., 2011; Szekeres et al., 2017; Reina et al., 2018).

67 The increasing consumption of imipenem inevitably entails environmental release of
68 cilastatin. Although, the photochemical fate (Reina et al., 2018) and treatment (Cabrera-Reina
69 et al., 2019) of imipenem have been the focus of past studies, very little is known on the
70 photochemical fate of cilastatin in water, and its treatment was only recently proposed as part
71 of an integrated advanced oxidation/reduction process for the degradation of
72 imipenem/cilastatin antibiotic aqueous solutions (Godini et al., 2019). However, detailed data
73 and discussion were not provided on the behavior/performance of cilastatin undergoing this
74 process.

75 This contribution aims to explore for the first time the photolytic fate of cilastatin in water
76 under 254-nm irradiation. Initially, ultra-pure water was used as matrix to study the effects of
77 concentration, pH, presence of t-butanol and humic acids on the cilastatin
78 (photo)transformation rate. Building on this knowledge, the photolysis of cilastatin spiked to
79 tap water, river water and wastewater effluent was monitored as a function of irradiation time.
80 At all times, modeling results are presented to confirm suggested hypotheses and discussion
81 on experimental data.

82

83 **2. Material and Methods**

84 ***2.1. Chemicals and samples***

85 Cilastatin sodium salt (purity grade ≥99.8%) was purchased from Sigma-Aldrich (Steinheim,
86 Germany). All organic solvents used were LC/MS grade. t-Butanol (≥99%) was supplied by
87 Fisher Chemicals (Pittsburgh, Pennsylvania). Analytical grade formic acid and humic acid
88 were supplied by Fluka Chemie GmbH (Bucks, Switzerland). Aqueous solutions of sodium

89 hydroxide (Fluka Chemie GmbH) or buffer solutions were used to adjust the pH value of the
90 irradiated solutions. The following chemicals were used to prepare the buffer solutions:
91 glacial acetic acid and boric acid (99.8%) supplied by Merck, KGaA (Darmstadt, Germany),
92 potassium phosphate dibasic trihydrate (≥99.0%) from Sigma-Aldrich (Steinheim, Germany),
93 sodium acetate trihydrate (≥99.5%) and potassium dihydrogen phosphate (≥99.5%), both
94 supplied by Fluka Chemie GmbH (Germany).
95 An EASYpure RF water purification system supplied by Barnstead/Thermolyne Corporation
96 (Dubuque, IA, USA) was used to prepare ultra-pure water. The matrix effect on cilastatin
97 photolysis was studied using: *(i)* freshwater sampled from the river Koiliaris at Kyani Akti
98 (Kalyves, Crete, Greece); *(ii)* tap water from the University campus (Chania, Crete, Greece),
99 and *(iii)* secondary treated wastewater effluent (WW) from the municipal wastewater
100 treatment plant of Chania (Crete, Greece), serving approximately 70,000 inhabitants. See
101 **Table A.1** in the Appendix for the chemical composition of the three water types used in this
102 work. Samples were collected the day before conducting the photo-experiments, and were
103 stored in the dark at 4 °C. All samples were initially analyzed and found free of cilastatin.
104
105 ***2.2. Photolysis experiments***
106 For all photolysis experiments, a home-made laboratory photoreactor (28.0 cm height × 28.4
107 cm length × 28.0 cm width) was used. The photoreactor was equipped with two 8 W low-
108 pressure mercury lamps having a strong emission line at 254 nm (Osram 8W G8 T5), each
109 mounted on an opposing sidewall of the photoreactor. The distance between each lamp and
110 the quartz vial used in the experiments was 13 cm. The rate of the incident UV light intensity
111 entering the solution (I_o, given in E L^{-1} s^{-1}, where E = Einstein) was determined using H_2O_2
112 as chemical actinometer, and was $I_o = (6.24 \pm 0.19) \times 10^{-6}$ E L^{-1} s^{-1}.

113 Aqueous solutions of cilastatin (CIL) were prepared daily by transferring the appropriate
114 volume from a 7 g L^{-1} methanolic stock solution to a tailor-made quartz vial (2.4 cm outer
115 diameter × 5.2 cm height). A gentle nitrogen stream was then applied to the headspace and,
116 after complete evaporation of methanol, 9 mL of water were added (ultra-pure H_2O, H_2O with
117 additives, tap water, natural water or WW effluent, depending on the experiment). The
118 mixture was then sonicated for a short time to facilitate CIL solubilization. The quartz vial
119 containing this aqueous solution was then capped and submitted to UV irradiation for the
120 preset time under mild magnetic agitation. The inner diameter of the quartz vial (2.0 cm) was
121 used as the optical path length of radiation. Blank experiments were also conducted by
122 placing the water samples inside the photoreactor with the lamps switched off. CIL removal
123 in the dark was below the error of the analytical method (varied between 0.1 and 2.6%) after
124 60 min, confirming that changes in the analytical signal after photolytic treatment were due to
125 photochemical processes only. All experiments were run at least in duplicates.
126
127 ***2.3 Analytical methods***
128 The absorbance of aqueous samples at 254 nm was measured using a single-beam UV-visible
129 spectrophotometer (UVmini-240, Shimadzu, Tokyo Japan), equipped with quartz cuvettes
130 having a 1 cm optical path length. The total organic carbon (TOC) content of water solutions
131 was measured using a TOC-5000 analyzer (Shimadzu, Kyoto, Japan; catalytic oxidation on Pt
132 at 680°C). The calibration was performed using standards of potassium phthalate.
133 All liquid chromatography/mass spectrometry (LC/MS) analyses on CIL were carried out
134 using an Agilent 1200 Series high-performance liquid chromatography (HPLC) system
135 equipped with a binary pump, autosampler, degasser and thermostated column compartment,
136 coupled to a diode array detector (DAD; the CIL analytical wavelength was 200 nm), and to
137 an Agilent 6110 single quadrupole MS system equipped with a multimode ionization source.

A Thermo-Electron Betasil C18 column (Waltham, MA, USA) of dimensions 2.1 mm ID × 100 mm length with 5 μm particle size was used for separation. The mobile phase consisted of 85% of water containing 0.1% formic acid and of 15% of acetonitrile containing 0.1% formic acid. The flow rate of the mobile phase was 250 μL min^{-1}, and the total analysis time was 10 min. For analysis, 60 μL of the sample were added to 100 μL polypropylene inserts and placed in 2 mL polypropylene autosampler vials equipped with caps, all purchased from Agilent (Palo Alto, USA). The injection volume was 20 μL. The MS conditions were: drying gas flow, 5 L min^{-1}; drying gas temperature, 350 °C; nebulizer pressure, 40 psi; collector capillary voltage, 2.0 kV; fragmentor voltage, 70 V; scan range (m/z), 100-1000 amu. The mass spectrometry data were recorded using the positive electrospray ionization (ESI) mode. The linearity of the method was tested using five concentration levels ranging from 1 to 100 mg L^{-1} (correlation coefficient r^2=0.9982). A 1.3 mg L^{-1} limit of quantification (LOQ) was estimated. This concentration level was not sufficiently to monitor the photolysis of 2.5 mg L^{-1} CIL (*i.e.*, 7×10^{-6} M). To increase sensitivity in these experiments, 100 μL of the irradiated sample were added to 250 μL vial inserts instead, the injection volume was set at 60 μL, and the 350-365 amu mass spectrometry signal was used to monitor changes in CIL concentration. The linearity of this method was assessed using a five-point calibration curve in the concentration range 0.5-5 mg L^{-1} and the estimated LOQ was 0.36 mg L^{-1}, which was sufficient for monitoring close to 85% CIL conversion. The linearity of the method was tested in each water matrix studied here and it was concluded that the matrix did not affect the analytical performance of the method.

3. Results and Discussion

3.1. Photodegradation kinetics

CIL undergoes several acid-base equilibria, which are described by the acid dissociation constants pK_{a1} = 2.0, pK_{a2} = 4.4 and pK_{a3} = 9.2 (Drugbank, 2020). These data allow for the distribution of the different species to be derived as a function of pH (Nourmoradi et al., 2019). In particular, the species' fractions α can be obtained as follows from the deprotonation equilibria:

$$\alpha_{H_3A^+} = \frac{[H^+]^3}{[H^+]^3 + K_{a1}[H^+]^2 + K_{a1}\,K_{a2}[H^+] + K_{a1}\,K_{a2}\,K_{a3}} \quad (1)$$

$$\alpha_{H_2A} = \frac{K_{a1}[H^+]^2}{[H^+]^3 + K_{a1}[H^+]^2 + K_{a1}\,K_{a2}[H^+] + K_{a1}\,K_{a2}\,K_{a3}} \quad (2)$$

$$\alpha_{HA^-} = \frac{K_{a1}\,K_{a2}[H^+]}{[H^+]^3 + K_{a1}[H^+]^2 + K_{a1}\,K_{a2}[H^+] + K_{a1}\,K_{a2}\,K_{a3}} \quad (3)$$

$$\alpha_{A^{2-}} = \frac{K_{a1}\,K_{a2}\,K_{a3}}{[H^+]^3 + K_{a1}[H^+]^2 + K_{a1}\,K_{a2}[H^+] + K_{a1}\,K_{a2}\,K_{a3}} \quad (4)$$

Note that H_3A^+ is the form of CIL with the amino and the two carboxylic groups all protonated, and the progressive deprotonation of these groups yields H_2A, HA^- and A^{2-}. The distribution of the different CIL forms as a function of pH is reported in **Fig. A.1** in the Appendix. It can be observed that HA^- strongly prevails at pH 6-8, *i.e.*, in the conditions around neutrality that are most often found in water treatment.

A first series of degradation experiments was carried out at pH 7, for concentration values of CIL ranging from 2.5 to 100 mg L^{-1} (note that 100 mg L^{-1} correspond to 2.6×10^{-4} M). The 2.5 mg L^{-1} concentration represented the lowest concentration level where conversion of up to 90% of the irradiated samples could be successfully monitored and quantified by the analytical instrumentation. The time evolution of CIL (**Fig. 1**) shows that degradation was

more effective as the initial concentration was lower. Data fitting of the concentration profiles from **Fig. 1** to $C_t = C_o\, e^{-kt}$ gave the k values used to compute the initial degradation rates R_0 (*vide infra*) shown in the inset graph, which increased with increasing C_o, from 2.2×10^{-8} M s^{-1} at 2.5 mg L^{-1} to 2.5×10^{-7} M s^{-1} at 100 mg L^{-1}.

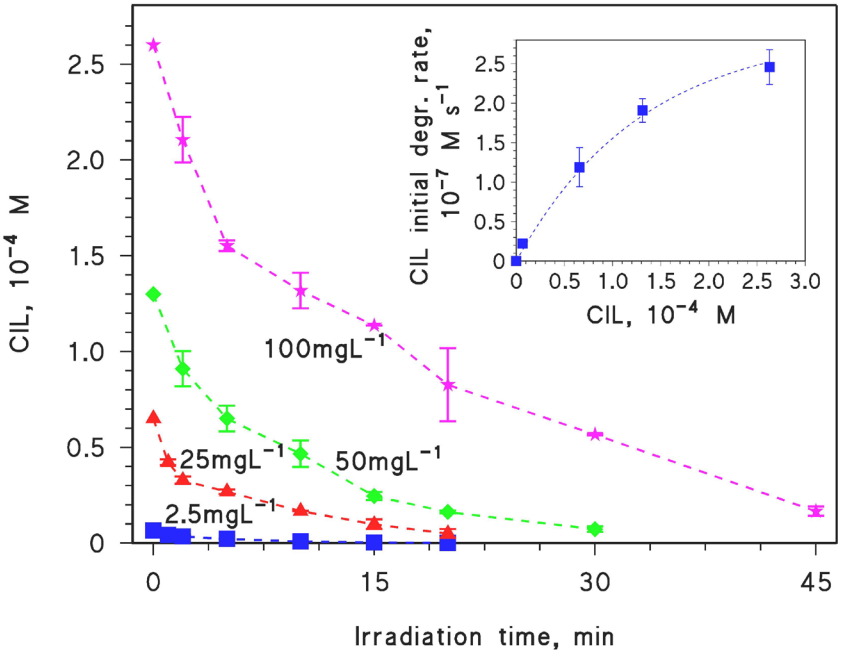

Fig. 1. Time trends of CIL concentration upon 254-nm irradiation at different initial concentration values, under ~neutral conditions (pH ~ 7). Data points are linked with dashed lines to visualize trends. **Inset:** initial degradation rates ($R_o = k\ C_o$) for the different concentrations examined here (C_o). The dashed connecting curve represents data fit with **Eq. (5)**. Some error bars are too small to be visible.

In a pseudo-first order approximation the initial degradation rate R_0 can be obtained as $R_0 = k\ C_0$, and the R_0 *vs*. C_0 trend is reported in the inset of **Fig. 1**. The observed increase with plateau may suggest that the substrate absorbs radiation and gets photolyzed as a consequence, up to saturation of absorption (Kourounioti et al., 2019; Alberti et al., 2021).

The monochromatic irradiation set-up allows for a simple Lambert-Beer approach to be applied, where the initial degradation rate can be expressed as follows (Braslavsky, 2007):

$$R_o = \gamma \left[1 - 10^{-\varepsilon_{CIL}\, b\, C_o}\right] \quad (5)$$

where γ is a constant proportionality factor, ε_{CIL} is the molar absorption coefficient of CIL at 254 nm, b = 2 cm the optical path length in solution, and C_o the initial CIL concentration. The experimental values of k and R_o in the different experiments conducted in this work are listed in **Table A.2** in the Appendix.

Independent spectrophotometric measurements gave ε_{CIL}(254 nm) = 1660 L mol^{-1} cm^{-1} at pH 7 (molar absorption of the HA^- species, see **Fig. A.1** in the Appendix). Therefore, by introducing in **Eq. (5)** all the known parameters it is possible to fit the experimental data of **Fig. 1** (insert) with γ as the only free-floating variable. The good fit results show that the phenomenon of absorption saturation indeed accounts for the plateau trend of R_0 *vs*. C_0.

In an attempt to identify the transformation products formed, the photolysis of 100 mg L^{-1} CIL solutions was monitored for 60 min, that is 15 min longer than the time required to remove CIL itself. During LC-MS analysis, the elution of several photoproducts was recorded. However, considering the parent compound, the use of a single quadrupole mass spectrometer could not provide a large amount of structural information, and specificity was limited compared to other more sophisticated types of mass spectrometers such as tandem quadrupole mass spectrometers (Kourounioti et al., 2019; Petrovic et al., 2007). Moreover, co-elution of products formed further obstructed their identification. The only photoproduct that could be tentatively identified was P375 at $[M\text{-}H]^+$=375 m/z, where the sulfide moiety of CIL was oxidized to a sulfoxide group. In the Appendix, **Fig. A.2** depicts the tentative

mechanism and **Table A.3** gives the sumary of analytical characteristics. P375 appeared after exposing CIL to 254-nm radiation for 10 min and reached its maximum at 45 min. The amount of organics remaining in the system after complete conversion of CIL was also evaluated, by measuring the TOC of 15 mg L^{-1} CIL water solutions before irradiation and for up to 240 min of UV_{254} exposure, after which time only ~10% TOC removal was recorded. This observation pointed towards the formation and accumulation of degradation products during irradiation, which were more recalcitrant than the parent compound (Yazdanbakhsh et al., 2018).

Another series of experiments studied the effect of pH on CIL degradation. The relevant time trends (see **Fig. 2**) suggest that degradation was faster at low pH and slowed down as the pH increased. A change in pH modifies the prevailing species that occur in solution, and the pH effect is most likely explained by different photochemical reactivity. The experimental degradation rate can be expressed as the sum of the contributions of the different species, each weighted for the relevant fraction, as follows:

$$R_o = \alpha_{H_3A^+} R_{H_3A^+} + \alpha_{H_2A} R_{H_2A} + \alpha_{HA^-} R_{HA^-} + \alpha_{A^{2-}} R_{A^{2-}} \quad (6)$$

where $\alpha_{H_3A^+}$, α_{H_2A}, α_{HA^-} and $\alpha_{A^{2-}}$ are expressed as per **Eqs. (1-4)** and are reported in **Fig. A.1** in the Appendix.

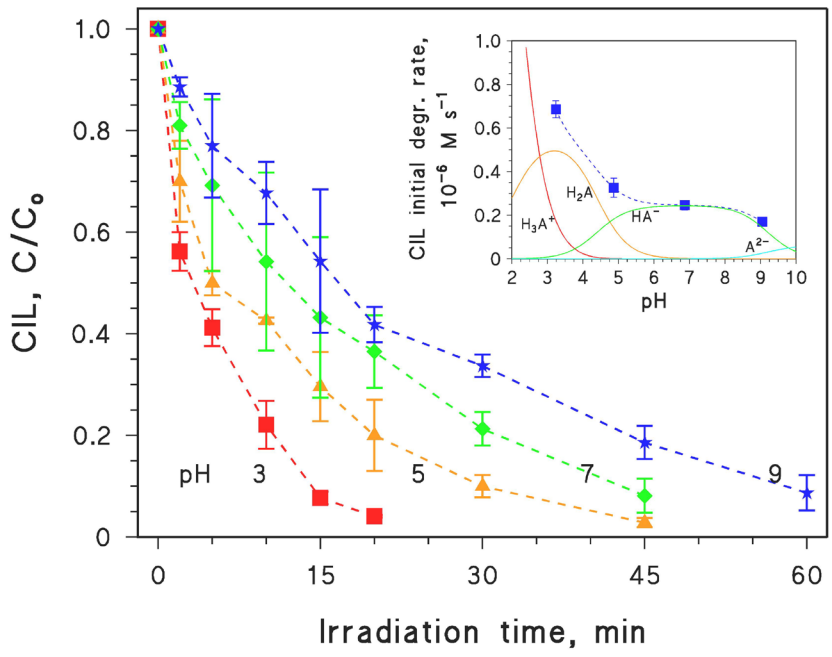

244

245 **Fig. 2.** Time trends of CIL (C_0 = 100 mg L^{-1} or 2.6×10^{-4} M) upon 254-nm irradiation, as a
246 function of pH. Data points are linked with dashed lines to visualize trends**. Inset:** trend of R_0
247 (initial degradation rate of CIL) *vs*. pH. The solid blue squares are the experimental data, the
248 dashed curve is the data fit with **Eq. (6)**, using $R_{H_3A^+}$, R_{H_2A}, R_{HA^-}, $R_{A^{2-}}$ as free-floating
249 parameters. The solid curves represent the contributions to photodegradation of the different
250 CIL species. Some error bars are too small to be visible.

251

252 The trend of R_0 *vs*. pH is shown in the inset of **Fig. 2**, and the experimental data (solid
253 squares) were fitted with **Eq. (6)** using $R_{H_3A^+}$, R_{H_2A}, R_{HA^-} and $R_{A^{2-}}$ as floating parameters.
254 The fit (see dashed curve in **Fig. 2**, inset) yielded $R_{H_3A^+} > R_{H_2A} > R_{HA^-} > R_{A^{2-}}$, which
255 accounts for the observed pH trend. The contributions of the different CIL species to
256 photodegradation (respectively, $\alpha_{H_3A^+}R_{H_3A^+}$, $\alpha_{H_2A}R_{H_2A}$, $\alpha_{HA^-}R_{HA^-}$ and $\alpha_{A^{2-}}R_{A^{2-}}$) are also
257 reported in the inset of **Fig. 2**, as solid curves as a function of pH. Notably, degradation at pH
258 6-8 would mainly be accounted for by HA$^-$, and its kinetics is not expected to vary much in
259 that pH interval.

The rate data derived for the different species ($R_{H_3A^+}$, R_{H_2A}, R_{HA^-} and $R_{A^{2-}}$) allow for the calculation of the relevant direct photolysis quantum yields. For a generic species *x* undergoing monochromatic 254-nm irradiation, the following relationship holds between the degradation rate R_x and the molar absorption coefficient at 254 nm, ε_x(254nm):

$$R_x = \Phi_x I_o (1 - 10^{-\varepsilon_x(254nm) b C_o}) \quad (7)$$

where *x* = H_3A^+, H_2A, HA^- or A^{2-}, Φ_x is the direct photolysis quantum yield for the *x* species, I_o = (6.24± 0.19) × 10^{-6} E L^{-1} s^{-1} the incident photon flux, *b* = 2 cm the optical path length, and the concentration C_o = 2.6×10^{-4} M (note that R_x is the contribution of the species *x* to the photodegradation of CIL when its molar fraction α_x = 1, thus we could use C_x = C_o). The absorbance of CIL was measured spectrophotometrically at 254 nm and at different pH values, and the experimental data of the molar absorption coefficients ε_{CIL}(254nm) are reported in **Fig. 3** as a function of pH (solid squares). The pH trend of ε_{CIL}(254nm) is accounted for by fact that the different CIL species have different absorption coefficients ε_x(254nm). Therefore, the experimental data can be fitted with the following equation:

$$\varepsilon_{CIL} = \alpha_{H_3A^+} \varepsilon_{H_3A^+} + \alpha_{H_2A} \varepsilon_{H_2A^+} + \alpha_{HA^-} \varepsilon_{HA^-} + \alpha_{A^{2-}} \varepsilon_{A^{2-}} \quad (8)$$

where all the molar absorption coefficients are referred to 254 nm. The fit of the ε_{CIL} experimental data with **Eq. (8)**, using $\varepsilon_{H_3A^+}$, ε_{H_2A}, ε_{HA^-} and $\varepsilon_{A^{2-}}$ as floating parameters, yielded the values of the 254-nm molar absorption coefficients of H_3A^+, H_2A, HA^- and A^{2-} that are reported in **Table A.4** in the Appendix. With these values and those of R_x it is possible to obtain the direct photolysis quantum yields of the various species at 254 nm, using

the relationship reported in **Eq. (7)**. The quantum yield data thus calculated are reported in **Table A.4** in the Appendix as well, and they follow the order $\Phi_{H_3A^+} > \Phi_{H_2A} > \Phi_{HA^-} > \Phi_{A^{2-}}$.

The quantum yield value of H_3A^+ is remarkably high, which explains why H_3A^+ undergoes faster photodegradation compared to H_2A (**Fig. 2**), although it absorbs radiation at a somewhat lesser extent (**Fig. 3**).

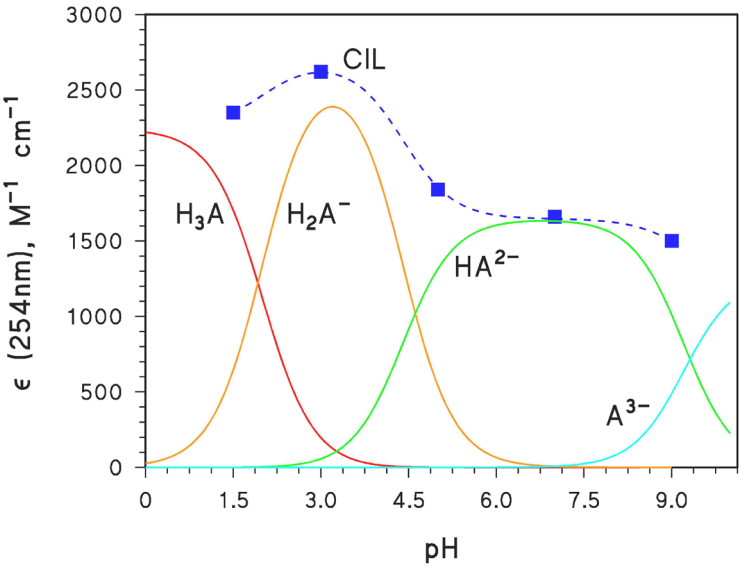

Fig. 3. Molar absorption coefficients (254 nm) of CIL and its different species, as a function of pH. The solid squares are the experimental data; the dashed curve is the data fit with **Eq. (8)**, using $\varepsilon_{H_3A^+}$, ε_{H_2A}, ε_{HA^-}, and $\varepsilon_{A^{2-}}$ as floating parameters; the solid curves represent the contributions to radiation absorption of the different CIL species (given by the respective products $\alpha_{H_3A^+}\varepsilon_{H_3A^+}$, $\alpha_{H_2A}\varepsilon_{H_2A}$, $\alpha_{HA^-}\varepsilon_{HA^-}$, and $\alpha_{A^{2-}}\varepsilon_{A^{2-}}$).

3.3. Effect of dissolved species

In some cases, the direct photolysis of organic molecules follows a self-sensitized pathway where the excited state of a compound is involved in the degradation of the same compound in the ground state. The occurrence of a bimolecular reaction between excited and ground

states ensures that the process kinetics becomes faster as the concentration C_0 increases (Bedini et al., 2012). In such cases the trend of R_0 *vs*. C_0 would not follow absorption saturation, and the latter should underestimate the degradation kinetics at high C_0. The data reported in the inset of **Fig. 1** show that degradation kinetics in our study strictly adhered to the absorption saturation model. Therefore, a self-sensitized process can be excluded. The same data rule out as well the opposite phenomenon, that ground-state CIL quenches the excited states of the same molecule. Indeed, in such cases one expects R_0 to grow more slowly with C_0 compared to the case of absorption saturation, sometimes yielding a trend with a maximum (Minto et al., 1989). The experimental data of **Fig. 1** rather suggest that CIL follows direct photolysis triggered by evolution of the excited state(s), excluding important interactions between these and the ground state.

In some relatively rare circumstances, the irradiation of a molecule in water can trigger $^{\bullet}$OH production. This happens for instance if the excited state is able to oxidize water (Sur et al., 2011), and in such cases photogenerated $^{\bullet}$OH could contribute to the degradation process. Such a hypothesis can be checked by addition of $^{\bullet}$OH scavengers to the irradiated system. t-butanol is a common and rather selective $^{\bullet}$OH scavenger that can be useful to this purpose (Buxton et al., 1988; Neta et al., 1988; Tsiampalis et al., 2019; Stathoulopoulos et al., 2020). As shown in **Fig. A.3** in the Appendix, the addition of 100 mg L^{-1} t-butanol had very little effect on CIL degradation, thereby suggesting that the transformation process does not involve $^{\bullet}$OH to a significant degree. It is noted that the experimental data obtained with alcohols should be treated with caution, because sometimes alcohols scavenge reactive states rather than $^{\bullet}$OH (Vione et al., 2010). However, in the present case the alcohol had a minor effect that suggests a limited importance of both $^{\bullet}$OH production and the possible confounding process (in contrast, the finding that t-butanol inhibits photolysis would not necessarily prove that the process involves $^{\bullet}$OH).

Natural water components can affect photodegradation either by competing with the substrate for the incoming photons, or by sensitizing its transformation (Canonica and Freiburghaus, 2001). Differently from the case of self-sensitization, in this indirect photochemical path the excited state of another compound (i.e. the photosensitizer) triggers degradation by reacting with the ground-state substrate (McNeill and Canonica, 2016). Actually, while competition for lamp irradiance by other compounds inhibits degradation, the sensitization process favors it.

Humic substances are major light absorbers and photosensitizers in surface waters (Rosario-Ortiz and Canonica, 2016), thus they are very suitable compounds with which to test the inhibition/sensitization potential. The presence of humic compounds at environmental concentrations (2.5 mg L^{-1}) inhibited the photodegradation of CIL as shown in **Fig. 4**. This result suggests that humic acids can act as radiation absorbers, thereby inhibiting the direct photolysis of the substrate, and that this inhibition process prevails over photosensitization (*vide infra* for additional calculations over this issue).

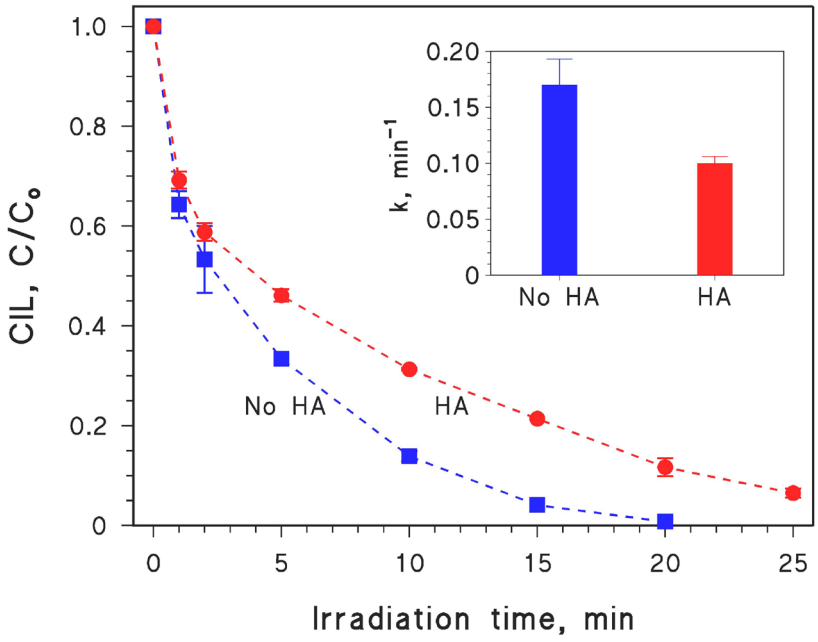

Fig. 4. Time trends of 2.5 mg L^{-1} CIL upon 254-nm irradiation at near-neutral pH, alone and upon addition of 2.5 mg L^{-1} humic acids (HA). Data points are linked with dashed lines to visualize trends. **Inset:** pseudo-first order photodegradation rate constants, together with their sigma-level error bounds. Some error bars are too small to be visible.

3.4. CIL photodegradation in real water matrices

In addition to humic substances, other components (organic and inorganic) that occur in natural waters might affect (either inhibit or enhance) the photodegradation kinetics of CIL. Therefore, photodegradation experiments were also carried out in the presence of natural water and treated wastewater samples spiked with CIL. The results of these experiments are shown in **Fig. 5**. Similar transformation rates were obtained in ultra-pure (Milli-Q quality) and tap water, while inhibition of CIL photodegradation was observed in river water and WW effluent. The recorded decrease in degradation kinetics with increasing matrix complexity, signified the importance of the organic and inorganic constituents typically found in natural waters and wastewaters.

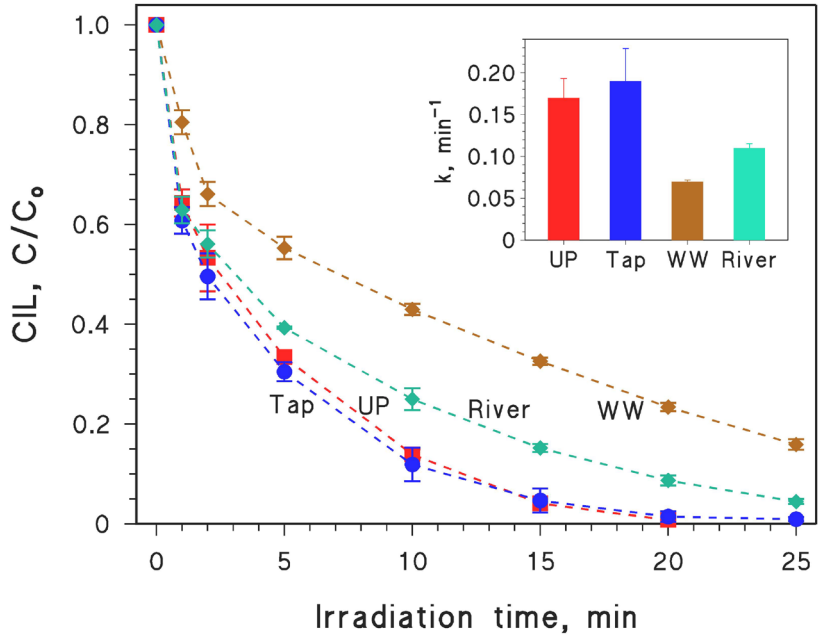

357

358 **Fig. 5.** Time trends of 2.5 mg L^{-1} CIL upon 254-nm irradiation in different water matrices:
359 ultra-pure water (UP), tap water (Tap), treated wastewater (WW) and river water (River).
360 Data points are linked with dashed lines to visualize trends. **Inset:** respective pseudo-first
361 order photodegradation rate constants, together with their sigma-level error bounds. Some
362 error bars are too small to be visible.

363

364 The absorption of radiation by CIL at concentration C_0 (in our case, C_0 = 2.5 mg L^{-1} that
365 corresponds to 7 × 10^{-6} M) in solution can be expressed as the absorbed photon flux $P_{a,CIL}$ [E
366 L^{-1} s^{-1}], which reads as follows according to the Lambert-Beer law (Braslavsky, 2007):

367

368 $$P_{a,CIL} = I_o\,[1-10^{-\varepsilon_{CIL}(254nm)\times b\times C_o}] \qquad (9)$$

369

370 where I_0 = 6.24 × 10^{-6} E L^{-1} s^{-1} is the incident photon flux from the lamp, ε_{CIL}(254nm) =
371 1660 L mol^{-1} cm^{-1} the molar absorption coefficient of CIL (HA^-) at the specified wavelength
372 and pH 7, b = 2 cm the optical path length, and C_0 = 7 × 10^{-6} M the initial CIL concentration.

Eq. (9) holds if CIL is the only light-absorbing species in solution. In the presence of other light-absorbing compounds (Sheikhmohammadi et al., 2019), the photon flux absorbed by CIL gets modified as follows (Braslavsky, 2007):

$$P'_{a,CIL} = I_o \frac{\varepsilon_{CIL}(254nm) \times C_o}{A_W(254nm)} [1 - 10^{-A_W(254nm) \times b}] \quad (10)$$

where A_w(254nm) [cm^{-1}] is the 254-nm absorbance of the water matrix spiked with CIL (in the present case, HA solution, tap water, river water or wastewater). In particular, it was A_w(254nm) = 0.073 cm^{-1} for 2.5 mg L^{-1} HA, 0.034 cm^{-1} for tap water, 0.061 cm^{-1} for river water, and 0.240 cm^{-1} for wastewater.

If the water matrix only affected radiation absorption by CIL, leaving its direct photolysis quantum yield unchanged, one would expect the CIL photolysis kinetics to be directly proportional to $P_{a,CIL}$. The trend of k (pseudo first-order photodegradation rate constant) as a function of $P_{a,CIL}$ is reported in **Fig. 6** for the different samples, where the dashed line shows the trend that would be expected at constant photolysis quantum yield. It is clearly shown that only tap water follows a comparable trend as ultra-pure water, while the other water matrices and the sample containing HA feature lower quantum yields for the direct photolysis of CIL (the relevant data points are unequivocally located below the dashed line, even when accounting for the experimental uncertainty). This finding suggests that the natural water components may on the one hand compete with CIL for the lamp irradiance; on the other hand, they do not behave as photosensitizers (in which case the relevant data points should be located above the dashed line) but rather inhibit the direct photolysis of CIL. Such a phenomenon of direct photolysis inhibition has already been observed in the presence of a range of natural organic compounds including humic substances (Vione et al., 2010; Liu et

al., 2020), and might involve either the physical quenching of CIL excited states (which would be quenched back to the ground state, inhibiting photolysis), or the back-reduction to CIL of partially oxidized degradation intermediates such as radicals or radical cations. The back-reduction effect could be triggered by the anti-oxidant (mostly phenolic) moieties that are ubiquitous in both HA and the natural organic matter (Wenk and Canonica, 2012).

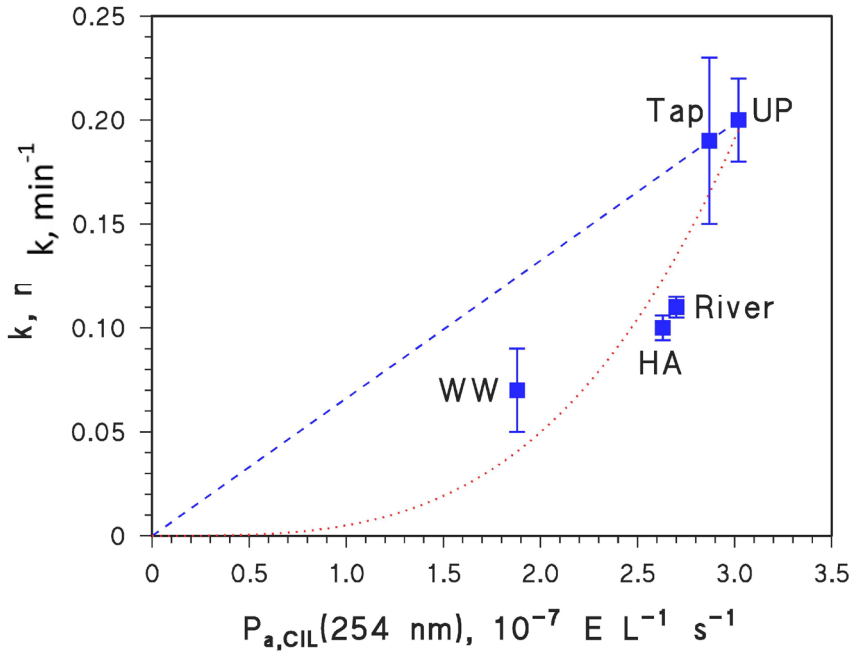

Fig. 6. Correlation between the pseudo-first order rate constant of CIL degradation (k) and the photon flux absorbed by CIL in solution ($P_{a,CIL}$). The dashed line shows the trend that would be expected if the water matrix (UP = ultra-pure water; Tap = tap water; HA = humic acids; River = river water; WW = wastewater) only acted as radiation absorber. The error bounds represent the sigma-level uncertainty deriving from the exponential fit of the time trend data, while the dotted curve is the result of data fit with a power function ($k = \alpha\ (P_{a,CIL})^{\beta}$).

411 ## 4. Conclusions

412

413 The rising global consumption of antibiotics resulted in the widespread occurrence of
414 antibiotic formulations in the aquatic environment. Although past investigations report the
415 photolytic behavior of antibiotics, they overlook studying the entailed problem of co-
416 administered agents released in water bodies. This is the first contribution studying in depth
417 the direct photolysis of cilastatin, a co-administered agent for the antibiotic imipenem, under
418 254-nm irradiation. The experimental data showed fast depletion of cilastatin in water under
419 UVC, and suggested that the direct photolysis of cilastatin is an efficient degradation
420 technique. Our experimental and modelling data demonstrated that degradation proceeded
421 faster at low pH values, thereby suggesting that altering the pH can synergistically accelerate
422 degradation kinetics. Moreover, we showed that the transformation process does not involve
423 $^{\bullet}OH$ to a significant degree, and that radiation absorbers may slow down degradation kinetics.
424 Finally, degradation rates decreased with increasing matrix complexity (tap water ~ ultra-pure
425 water > river water > wastewater effluent), suggesting that the natural water components may
426 both compete with cilastatin for the 254 nm photon absorption and decrease its direct
427 photolysis quantum yield. Nonetheless, cilastatin depletion in complex matrices can be
428 completed within reasonable exposure times.

429

References

Alberti, S., Sotiropoulou, M., Fernández, E., Solomou, N., Ferretti, M., Psillakis, E., 2021. UV-254 degradation of nicotine in natural waters and leachates produced from cigarette butts and heat-not-burn tobacco products. Environ. Res. 110695. https://doi.org/10.1016/j.envres.2020.110695

Bedini, A., De Laurentiis, E., Sur, B., Maurino, V., Minero, C., Brigante, M., Mailhot, G., Vione, D., 2012. Phototransformation of anthraquinone-2-sulphonate in aqueous solution. Photochem. Photobiol. Sci. 11, 1445. https://doi.org/10.1039/c2pp25111f

Braslavsky, S.E., 2007. Glossary of terms used in photochemistry, 3rd edition (IUPAC Recommendations 2006). Pure Appl. Chem. 79, 293–465. https://doi.org/10.1351/pac200779030293

Briones, A.A., Guevara, I.C., Mena, D., Espinoza, I., Sandoval-Pauker, C., Guerrero, L.R., Jentzsch, P.V., Bisesti, F.M., 2020. Degradation of meropenem by heterogeneous photocatalysis using TiO2 /fiberglass substrates. Catalysts 10, 3–5. https://doi.org/10.3390/catal10030344

Buxton, G. V., Greenstock, C.L., Helman, W.P., Ross, A.B., 1988. Critical Review of rate constants for reactions of hydrated electrons, hydrogen atoms and hydroxyl radicals ($^{\bullet}OH/^{\bullet}O^{-}$ in Aqueous Solution. J. Phys. Chem. Ref. Data 17, 513–886. https://doi.org/10.1063/1.555805

Cabrera-Reina, A., Martínez-Piernas, A.B., Bertakis, Y., Xekoukoulotakis, N.P., Agüera, A., Sánchez Pérez, J.A., 2019. TiO_2 photocatalysis under natural solar radiation for the degradation of the carbapenem antibiotics imipenem and meropenem in aqueous solutions at pilot plant scale. Water Res. 166, 115037. https://doi.org/https://doi.org/10.1016/j.watres.2019.115037

Canonica, S., Freiburghaus, M., 2001. Electron-rich phenols for probing the photochemical

reactivity of freshwaters. Environ. Sci. Technol. 35, 690–695. https://doi.org/10.1021/es0011360

Cheng, S.F., Lee, Y.C., Kuo, C.Y., Wu, T.N., 2015. A case study of antibiotic wastewater treatment by using a membrane biological reactor system. Int. Biodeterior. Biodegrad. 102, 398–401. https://doi.org/10.1016/j.ibiod.2015.04.018

Drugbank, 2020. https://go.drugbank.com/drugs/DB01597, last assessed: Decmber 2020.

Drusano, G.L., Standiford, H.C., Bustamante, C., Forrest, A., Rivera, G., Leslie, J., Tatem, B., Delaportas, D., MacGregor, R.R., Schimpff, S.C., 1984. Multiple-dose pharmacokinetics of imipenem-cilastatin. Antimicrob. Agents Chemother. 26, 715–721. https://doi.org/10.1128/AAC.26.5.715

Godini, H., Sheikhmohammadi, A., Abbaspour, L., Heydari, R., Khorramabadi, G.S., Sardar, M., Mahmoudi, Z., 2019. Energy consumption and photochemical degradation of Imipenem/Cilastatin antibiotic by process of UVC/ Fe 2+ / H 2 O 2 through response surface methodology. Optik (Stuttg). 182, 1194–1203. https://doi.org/10.1016/j.ijleo.2019.01.071

Hsieh, J.Y.K., Maglietto, B.K., Bayne, W.F., 1985. Separation identification, and quantification of n-acetyl cilastatin in human urine. J. Liq. Chromatogr. 8, 513–520. https://doi.org/10.1080/01483918508067097

Hutt, A.J., O'Grady, J., 1996. Drug chirality: A consideration of the significance of the stereochemistry of antimicrobial agents. J. Antimicrob. Chemother. 37, 7–32. https://doi.org/10.1093/jac/37.1.7

Klein, E.Y., Boeckel, T.P. Van, Martinez, E.M., Pant, S., Gandra, S., Levin, S.A., Goossens, H., Laxminarayan, R., 2018. Global increase and geographic convergence in antibiotic consumption between 2000 and 2015. Proc. Natl. Acad. Sci. 115, E3463–E3470. https://doi.org/10.1073/PNAS.1717295115

480 Kourounioti, E., Psillakis, E., Vione, D., 2019. UV-induced transformation of 2,3-dibromo-
481 5,6-dimethyl-1,4-benzoquinone in water and treated wastewater. Environ. Res. 175,
482 343–350. https://doi.org/10.1016/j.envres.2019.05.018
483 Kumarasamy, K.K., Toleman, M.A., Walsh, T.R., Bagaria, J., Butt, F., Balakrishnan, R.,
484 Chaudhary, U., Doumith, M., Giske, C.G., Irfan, S., Krishnan, P., Kumar, A. V,
485 Maharjan, S., Mushtaq, S., Noorie, T., Paterson, D.L., Pearson, A., Perry, C., Pike, R.,
486 Rao, B., Ray, U., Sarma, J.B., Sharma, M., Sheridan, E., Thirunarayan, M.A., Turton, J.,
487 Upadhyay, S., Warner, M., Welfare, W., Livermore, D.M., Woodford, N., 2010.
488 Emergence of a new antibiotic resistance mechanism in India, Pakistan, and the UK: a
489 molecular, biological, and epidemiological study. Lancet Infect. Dis. 10, 597–602.
490 https://doi.org/10.1016/S1473-3099(10)70143-2
491 Liu, Y., Mekic, M., Carena, L., Vione, D., Gligorovski, S., Zhang, G., Jin, B., 2020. Tracking
492 photodegradation products and bond-cleavage reaction pathways of triclosan using ultra-
493 high resolution mass spectrometry and stable carbon isotope analysis. Environ. Pollut.
494 264, 114673. https://doi.org/10.1016/j.envpol.2020.114673
495 McNeill, K., Canonica, S., 2016. Triplet state dissolved organic matter in aquatic
496 photochemistry: reaction mechanisms, substrate scope, and photophysical properties.
497 Environ. Sci. Process. Impacts 18, 1381–1399. https://doi.org/10.1039/C6EM00408C
498 Minto, R., Samanta, A., Das, P.K., 1989. Time-resolved nanosecond and picosecond
499 absorption studies of excited-state properties of 1-thiobenzoylnaphthalene. Can. J. Chem.
500 67, 967–972. https://doi.org/10.1139/v89-148
501 Neta, P., Huie, R.E., Ross, A.B., 1988. Rate constants for reactions of inorganic radicals in
502 aqueous solution. J. Phys. Chem. Ref. Data 17, 1027–1284.
503 https://doi.org/10.1063/1.555808
504 Norrby, S.R., Rogers, J.D., Ferber, F., Jones, K.H., Zacchei, A.G., Weidner, L.L.,

505 Demetriades, J.L., Gravallese, D.A., Hsieh, J.Y., 1984. Disposition of radiolabeled
506 imipenem and cilastatin in normal human volunteers. Antimicrob. Agents Chemother.
507 26, 707–714. https://doi.org/10.1128/AAC.26.5.707
508 Nourmoradi, H., Asgari, E., Sheikhmohammadi, A., Manshouri, M., 2019. Performance
509 intensification of BzP photo-catalytic degradation through adding exogenous oxidant.
510 Opt. J. Light Electron Opt. https://doi.org/10.1016/j.ijleo.2019.163571
511 Papp-Wallace, K.M., Endimiani, A., Taracila, M.A., Bonomo, R.A., 2011. Carbapenems:
512 Past, present, and future. Antimicrob. Agents Chemother.
513 https://doi.org/10.1128/AAC.00296-11
514 Petrovic, M., Petrovic, M., Barceló, D., 2007. LC-MS for identifying photodegradation
515 products of pharmaceuticals in the environment. TrAC - Trends Anal. Chem. 26, 486–
516 493. https://doi.org/10.1016/j.trac.2007.02.010
517 Proia, L., Anzil, A., Borrego, C., Farrè, M., Llorca, M., Sanchis, J., Bogaerts, P., Balcázar,
518 J.L., Servais, P., 2018. Occurrence and persistence of carbapenemases genes in hospital
519 and wastewater treatment plants and propagation in the receiving river. J. Hazard. Mater.
520 358, 33–43. https://doi.org/10.1016/j.jhazmat.2018.06.058
521 Reina, A.C., Martínez-Piernas, A.B., Bertakis, Y., Brebou, C., Xekoukoulotakis, N.P.,
522 Agüera, A., Sánchez Pérez, J.A., 2018. Photochemical degradation of the carbapenem
523 antibiotics imipenem and meropenem in aqueous solutions under solar radiation. Water
524 Res. 128, 61–70. https://doi.org/10.1016/j.watres.2017.10.047
525 Rosario-Ortiz, F.L., Canonica, S., 2016. Probe compounds to assess the photochemical
526 activity of dissolved organic matter. Environ. Sci. Technol. 50, 12532–12547.
527 https://doi.org/10.1021/acs.est.6b02776
528 Sheikhmohammadi, A., Yazdanbakhsh, A., Moussavi, G., Eslami, A., Rafiee, M., Sardar, M.,
529 Almasian, M., 2019. Degradation and COD removal of trichlorophenol from wastewater

using sulfite anion radicals in a photochemical process combined with a biological reactor: Mechanisms, degradation pathway, optimization and energy consumption. Process Saf. Environ. Prot. 123, 263–271. https://doi.org/10.1016/j.psep.2019.01.020

Stathoulopoulos, A., Mantzavinos, D., Frontistis, Z., 2020. Coupling persulfate-based AOPs: A novel approach for piroxicam degradation in aqueous matrices. Water (Switzerland) 12. https://doi.org/10.3390/W12061530

Sur, B., Rolle, M., Minero, C., Maurino, V., Vione, D., Brigante, M., Mailhot, G., 2011. Formation of hydroxyl radicals by irradiated 1-nitronaphthalene (1NN): oxidation of hydroxyl ions and water by the 1NN triplet state. Photochem. Photobiol. Sci. 10, 1817. https://doi.org/10.1039/c1pp05216k

Szekeres, E., Baricz, A., Chiriac, C.M., Farkas, A., Opris, O., Soran, M.L., Andrei, A.S., Rudi, K., Balcázar, J.L., Dragos, N., Coman, C., 2017. Abundance of antibiotics, antibiotic resistance genes and bacterial community composition in wastewater effluents from different Romanian hospitals. Environ. Pollut. 225, 304–315. https://doi.org/10.1016/j.envpol.2017.01.054

Tran, N.H., Chen, H., Reinhard, M., Mao, F., Gin, K.Y.H., 2016. Occurrence and removal of multiple classes of antibiotics and antimicrobial agents in biological wastewater treatment processes. Water Res. 104, 461–472. https://doi.org/10.1016/j.watres.2016.08.040

Tsiampalis, A., Frontistis, Z., Binas, V., Kiriakidis, G., Mantzavinos, D., 2019. Degradation of Sulfamethoxazole Using Iron-Doped Titania and Simulated Solar Radiation. Catalysts 9, 612. https://doi.org/10.3390/catal9070612

Vione, D., Khanra, S., Das, R., Minero, C., Maurino, V., Brigante, M., Mailhot, G., 2010. Effect of dissolved organic compounds on the photodegradation of the herbicide MCPA in aqueous solution. Water Res. 44, 6053–6062.

https://doi.org/10.1016/j.watres.2010.07.079

Wenk, J., Canonica, S., 2012. Phenolic antioxidants inhibit the triplet-induced transformation of anilines and sulfonamide antibiotics in aqueous solution. Environ. Sci. Technol. 46, 5455–5462. https://doi.org/10.1021/es300485u

Yazdanbakhsh, A., Eslami, A., Moussavi, G., Rafiee, M., Sheikhmohammadi, A., 2018. Photo-assisted degradation of 2, 4, 6-trichlorophenol by an advanced reduction process based on sulfite anion radical: Degradation, dechlorination and mineralization. Chemosphere 191, 156–165. https://doi.org/10.1016/j.chemosphere.2017.10.023

Yılmaz, Ç., Özcengiz, G., 2017. Antibiotics: Pharmacokinetics, toxicity, resistance and multidrug efflux pumps. Biochem. Pharmacol. 133, 43–62. https://doi.org/https://doi.org/10.1016/j.bcp.2016.10.005